COMMUNICATION

Check for updates

Lower limits for non-radiative recombination loss in organic donor/acceptor complexes†

Yun Liu, [iD][a] Zilong Zheng, [iD][bc] Veaceslav Coropceanu, [iD][bd] Jean-Luc Brédas [iD][bd] and David S. Ginger*[a]

Understanding the factors controlling radiative and non-radiative transition rates for charge transfer states in organic systems is important for applications ranging from organic photovoltaics (OPV) to lasers and LEDs. We explore the role of charge-transfer (CT) energetics, lifetimes, and photovoltaic properties in the limit of very slow non-radiative rates by using a model donor/acceptor system with photoluminescence dominated by thermally activated delayed fluorescence (TADF). This blend exhibits an extremely high photoluminescence quantum efficiency (PLQY = $\sim$22%) and comparatively long PL lifetime, while simultaneously yielding appreciable amounts of free charge generation (photocurrent external quantum efficiency EQE of 24%). In solar cells, this blend exhibits non-radiative voltage losses of only $\sim$0.1 V, among the lowest reported for an organic system. Notably, we find that the non-radiative decay rate, k_{nr}, is on the order of 10^5 s^{-1}, approximately 4–5 orders of magnitude slower than typical OPV blends, thereby confirming that high radiative efficiency and low non-radiative voltage losses are achievable by reducing k_{nr}. Furthermore, despite the high radiative efficiency and already comparatively slow k_{nr}, we find that k_{nr} is nevertheless much faster than predicted by Marcus–Levich–Jortner two-state theory and we conclude that CT-local exciton (LE) hybridization is present. Our findings highlight that it is crucial to evaluate how radiative and non-radiative rates of the LE states individually influence the PLQY of charge-transfer states, rather than solely focusing on the PLQY of the LE. This conclusion will guide material selection in achieving low non-radiative voltage loss in organic solar cells and high luminescence efficiency in organic LEDs.

Introduction

Donor–acceptor (D:A) blends are widely used in efficient organic light-emitting diodes (OLEDs) and organic

New concepts

The fate of charge-transfer (CT) states formed at donor/acceptor interfaces is central to the operation of organic optoelectronics. Making CT states more luminescent has advantages in both charge-generating and light-emitting applications. Recently, quantum mechanical mixing of CT states with local excitons (CT-LE mixing) has gained attention as a way to make the CT states brighter by allowing a ''dark'' CT state to borrow intensity from a ''bright'' LE state. This effect gains importance when the CT and LE energies are similar. However, we show that it is possible for CT states in wide-gap blends to have photoluminescence quantum yields (PLQYs) higher than those of the individual components. Even when the CT and LE energies are relatively dissimilar, the electronic coupling between the lowest lying LE state and the CT state is nevertheless still important and can dominate the non-radiative transition rate. In such cases, the PLQY of the CT state can be compromised by CT-LE mixing as the CT state acquires a faster non-radiative decay rate from the LE. Material selection for highly efficient CT-based OLEDs and large-gap organic solar cells thus requires scrutiny of not just the PLQY of the LE state, but also the individual radiative and non-radiative lifetimes.

photovoltaics (OPVs). Detailed balance arguments indicate that these two applications are two sides of the same coin,[1,2] which, as OPVs have climbed to higher efficiencies, has led to the realization in the organic solar cell community that OPVs should also be bright (radiatively efficient) if they are to approach theoretical efficiency limits.[3] Despite recent efforts to improve the luminescence efficiency of charge-transfer states, OPVs still largely suffer significant energy losses from non-radiative recombination[3-5] compared to inorganic systems like perovskites or GaAs.[6-9] Typically, polymer/fullerene-based OPVs have non-radiative voltage losses (ΔV_{OC}^{nr}) in the range of $\sim$0.3–0.4 V,[10] with the most efficient polymer/non-fullerene systems reaching ΔV_{OC}^{nr} of 0.2–0.3 V.[11-17] While these values approach those for commercial silicon ($\sim$0.18 V),[18] they still

[a] *Department of Chemistry, University of Washington, Seattle, WA, 98195-2120, USA. E-mail: dginger@uw.edu*

[b] *School of Chemistry and Biochemistry, Georgia Institute of Technology, Atlanta, Georgia, 30332-0400, USA*

[c] *College of Materials Science and Engineering, Beijing University of Technology, Beijing 100124, China*

[d] *Department of Chemistry and Biochemistry, The University of Arizona, Tucson, AZ, 85721-0088, USA*

compare poorly with ΔV_{OC}^{nr} values of 0.027 V for GaAs[8] and 0.034 V for emerging perovskite materials.[9] The so-called "energy gap law"[19] for non-radiative geminate recombination rates has been invoked to set the boundaries for the radiative efficiency of organic D:A blends. Furthermore, Vandewal and co-workers have suggested that organic blends should have intrinsically high non-radiative recombination rates due to the coupling of the electron transfer process with high-frequency intramolecular vibrations.[10] Multiple groups have highlighted the importance of controlling reorganization energy and disorder to achieve high radiative efficiency.[20–22] Despite these efforts, the radiative and non-radiative rates of organic (macro)molecules in OLEDs and OPVs are still not fully understood at the microscopic level. For example, remarkably emissive CT states have been reported with radiative efficiencies exceeding those predicted by the "energy gap law".[12,13,23,24] Along the same line, after it was demonstrated in 2012 that D:A exciplexes[25] can be used to build efficient OLEDs, there have been major advances in exciplex-based OLEDs with external quantum efficiencies (EQEs) of 20.0% for blue and 24.0% for green emitting devices.[26] Since many exciplex emitters rely on the thermally activated delayed fluorescence (TADF) mechanism, a significant amount of recent work was mainly focused on understanding intersystem crossing (ISC) and reverse ISC transitions. In contrast, understanding the transition rates of the exciplex or CT state itself has received less attention.

To gain insight into the radiative and non-radiative rates of the CT state as well as the impact of these rates on the optoelectronic performance, we use a model TADF-emissive blend composed of 4,4′,4″-tris[3-methylphenyl(phenyl)amino] triphenylamine (m-MTDATA) as the donor and tris-[3-(3-pyridyl) mesityl]borane (3TPYMB) as the acceptor. TADF blends, compared to typical donor/acceptor OPV blends, are luminescent systems with long PL lifetimes due to thermally activated reverse intersystem crossing from the lowest triplet state to the lowest singlet excited state.[27–30] The m-MTDATA/3TPYMB blend is intriguing because it exhibits both a high photoluminescence quantum yield (PLQY $\sim$ 22%) and an appreciable photovoltaic external quantum efficiency (EQE$_{PV}$ max $\sim$24%) for converting incident photons into photocurrent.[31–34] We find that the non-radiative decay rate is significantly faster than that predicted by the Marcus–Levich–Jortner (MLJ) two-state model within the realm of plausible molecular parameters. Combining our experimental and theoretical results, we conclude that hybridization of the CT states with the local exciton (LE) states speeds up the non-radiative decay and harms the photoluminescence quantum yield, leading to additional non-radiative recombination loss. Our results highlight the importance of controlling CT energetics, namely CT-LE hybridization, to achieve small non-radiative recombination loss in OPVs and high radiative efficiency in OLEDs.

Results

Photoluminescence properties

Fig. 1a shows the molecular structures and reported state energies of both m-MTDATA and 3TPYMB.[31] We deposited
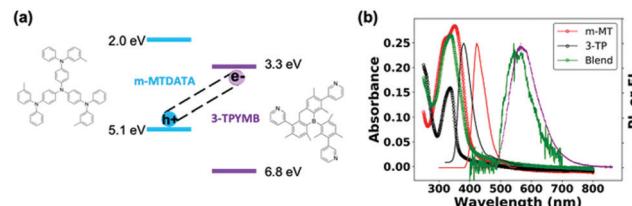
Fig. 1 (a) State energies[31] and molecular structures of m-MTDATA and 3TPYMB. (b) Absorption (-o-) and PL spectra (-) of neat donor (red), acceptor (black) and blend films/devices (green) overlaid with EL spectrum (purple) of the blend device. The PL spectrum of the blend was measured from the solar cell device stack.

(1 : 1) blend films of m-MTDATA:3TPYMB by thermal co-evaporation of the donor and acceptor materials. Fig. 1b shows the PL of the neat donor and acceptor materials, as well as the blend. Compared to neat donor and acceptor films, the m-MTDATA:3TPYMB blend shows a significantly red-shifted PL spectrum, consistent with charge-transfer state emission, indicating that charge and energy transfer from the local exciton to the CT state are highly efficient, in good agreement with previous reports.[31,32]

Fig. 2 shows the time-resolved photoluminescence (PL) from the blend measured at room temperature. We observe a clear bi-phasic PL decay with both prompt and delayed emission, characteristic of TADF materials. At 80 K, the delayed component slows down as thermally activated intersystem crossing, the rate-limiting step within this time range, is suppressed (Fig. S1, ESI†). Fig. 2 also shows fits of a bi-exponential decay to the observed PL kinetics, which yields lifetimes of 4.7 μs and 43 μs for the prompt and delayed decays, respectively. These values are consistent with previous reports on this system.[31,32,34] On glass substrates, our blends exhibit a PLQY from the CT state of 22%. This PLQY value is 2–3 orders of magnitude higher than typical CT emission in OPVs.[12,35] Based on our measured PLQYs and lifetimes, we determine the radiative (k_r), intersystem crossing (k_{ISC}), and non-radiative (k_{nr}) rate constants of the singlet CT state (^{1}CT) to
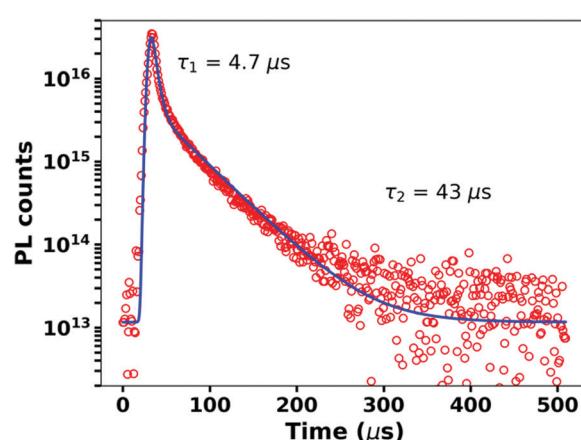

Fig. 2 Time-resolved PL decay of the m-MTDATA/3TPYMB blend (red circles) shows prompt and delayed emission with time constants of 4.7 μs and 43 μs. A bi-exponential function convolved with experimental IRF is fit to the data and shown in blue.

be $k_r = 2.75 \times 10^4 \text{ s}^{-1}$, $k_{ISC} = 8.9 \times 10^4 \text{ s}^{-1}$, and $k_{nr} = 9.8 \times 10^4 \text{ s}^{-1}$, respectively (see ESI,† Section S1 for details on the rate calculation). Compared to previously reported k_r and k_{nr} values for CT states in D/A OPV blends, the m-MTDATA/3TPYMB blend system exhibits what appears to be a remarkably slow non-radiative rate—roughly 5 orders of magnitude slower than commonly reported k_{nr} values for CT states (Table S1, ESI†).

Photovoltaic properties

Next, we explore the photovoltaic properties of the m-MTDATA: 3TPYMB blend. We chose the following device structure: glass/ ITO/PEDOT-PSS/MeO-TPD/m-MTDATA/m-TDATA:3TPYMB/3TPYMB/ Bphen/LiF/Al, in order to avoid formation of any potentially interfering exciplexes at the interfaces of the active layer and transport layers. The device demonstrates a maximum incident photon to charge collection efficiency (EQE$_{PV}$) of 24% (Fig. 3a). We measured the refractive indices *via* ellipsometry and modelled the absorption of the m-MTDATA:3TPYMB layer in the device (see Fig. S2, ESI†) using a transfer matrix algorithm to calculate the photovoltaic internal quantum efficiency (IQE$_{PV}$).[36] We find that IQE$_{PV}$ is over 40% over the region corresponding to the majority of the donor and acceptor absorption spectra. Fig. 3c shows the electroluminescence quantum yield (EQE$_{EL}$) measured as a function of injected current density. In the best performing PV cell, we measure EQE$_{EL}$ to be 1.67% at injection current equivalent to short-circuit current at 1 sun illumination condition (average EQE$_{EL}$ = 1.82 ± 0.02%, number of devices, $N = 6$). We thus obtain the corresponding ΔV_{OC}^{nr} according to eqn (2) below to be only ~ 100 meV, which places this system among the most emissive charge-generating organic photodiode structures, comparable to the best OLED-based OPVs reported so far (Fig. 3d).[10,12,13,15,16,24,37–42] Fig. 3b shows that under AM1.5G illumination conditions, the best performing PV cell yields a V_{OC} of 2.12 V (2.12 ± 0.03 V, $N = 6$); however, despite a photocurrent EQE$_{PV}$ of ~ 24%, J_{SC} only reaches ~ 0.1 mA cm^{-2} (0.09 ± 0.02 mA cm^{-2}, $N = 6$) due to the wide bandgap and consequent poor overlap with the solar spectrum.

The experimental V_{OC} of 2.12 V is 0.73 V lower than the Shockley–Queisser V_{OC} limit (V_{OC}^{SQ}) of 2.85 V for the bandgap of 3.239 eV. Thus, we next consider the factors governing the overall voltage loss in our CT-based TADF-emissive solar cell.

Following the well-established framework based on detailed balance,[43,44] we separate the V_{OC} loss into two sources: (1) charge generation loss (ΔV_{OC}^{SC}), which is due to non-ideal EQE$_{PV}$ and (2) charge recombination loss, both radiative and non-radiative, where ΔV_{OC} is related to energy loss due to non-radiative recombination (eqn (1)):

$$V_{OC} = V_{OC}^{SQ} + \Delta V_{OC}^{SC} + \Delta V_{OC}^{r} + \Delta V_{OC}^{nr} \quad (1)$$

$$q\Delta V_{OC}^{nr} = -kT\ln(\text{EQE}_{EL}) \quad (2)$$

The radiative voltage loss (ΔV_{OC}^{r}) is due to radiative recombination that is not accounted for in the Shockley–Queisser limit due to additional absorption/emission states below the bandgap (which is a step function in the ideal SQ case). By analyzing the sub-gap EQE and EL spectra within Rau's reciprocity framework (Table 1; see ESI,† Section S2 for details), we determine ΔV_{OC}^{r} to be -0.600 V. This value is on the higher end compared to efficient BHJ OPVs.[12–15,45] We attribute this large ΔV_{OC}^{r} to the large offset between E_{CT} and the bandgap (Fig. S3, ESI†), leading to significant below-gap absorption. Taken together, our voltage loss analysis (1) demonstrates a small non-radiative recombination loss, among the lowest reported to date in charge-generating organic solar cells and (2) highlights the challenge of simultaneously reducing radiative and non-radiative voltage losses in CT-based solar cells.[46]

Transition rates in the Marcus–Levich–Jortner framework

At this point, we return to analyze the k_{nr} values in more detail. It is instructive to compare the emissive properties of the m-MTDATA:3TPYMB blend with those of the m-MTDATA and 3TPYMB components. We measured the radiative rate (k_r^{LE}), non-radiative rate (k_{nr}^{LE}) and PLQY, respectively, to be $5.14 \times 10^7 \text{ s}^{-1}$, $4.2 \times 10^8 \text{ s}^{-1}$ and 11% in m-MTDATA, and $6.44 \times 10^7 \text{ s}^{-1}$, $8.97 \times 10^8 \text{ s}^{-1}$ and 6% in 3TPYMB (see ESI,† Section S3 for details). Interestingly, the PLQY of the blend (22%) is over twice as large as the respective values for the D and A components. Another intriguing finding is that the non-radiative rate of the CT state is about four orders of magnitude slower than the non-radiative rates of the related local-exciton (LE) states despite the fact that the CT state is located about 0.7 eV and 1.0 eV below the emissive states of m-MTDATA and 3TPYMB, respectively.
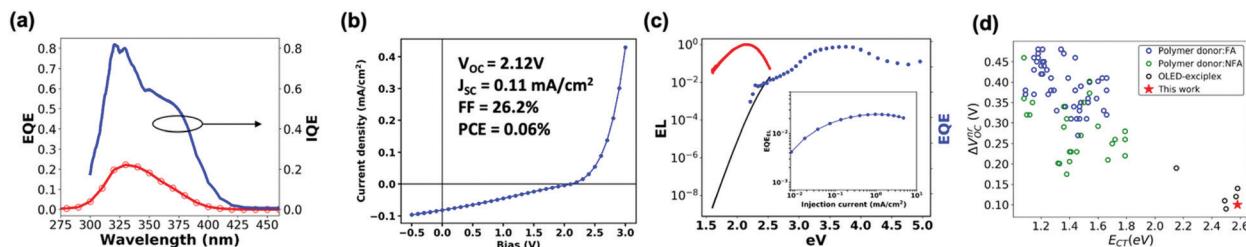

Fig. 3 (a) EQE$_{PV}$ and IQE$_{PV}$ spectra. (b) $J-V$ curve measured under simulated AM1.5G illumination. (c) EL (red) and EQE$_{PV}$ (blue) spectra and re-created EQE$_{PV}$ (black) spectrum based on Rau's reciprocity theorem. The EL spectrum is divided by the blackbody radiation spectrum and multiplied by a scaling factor to match the low-energy EQE tail. (inset) Electroluminescence external quantum efficiency (EQE$_{EL}$) measured at a range of injection current. (d) Survey of ΔV_{nr}^{OV} and E_{CT} of previously reported CT-based donor/acceptor blends (blue and green),[10,12,13,15,16,24,37–42] a previously reported OLED exciplex-based blend,[37] and our blend.

Table 1 Results of the open-circuit voltage loss analysis

E_{gap}	V_{OC}^{SQ}	ΔV_{OC}^{SC}	ΔV_{OC}^{r}	ΔV_{OC}^{nr}	V_{OC}^{calc}	V_{OC}^{meas}
3.239 eV	2.85 V	−0.0484 V	−0.6 V	−0.104 V	2.098 V	2.11 V

Therefore, it is of great interest (1) to examine in detail the radiative and non-radiative transition rates of the CT state and (2) to correlate the luminescence properties with the photovoltaic properties in order to understand whether a small non-radiative recombination loss is expected given the large bandgap in our system.

The radiative and non-radiative transitions involving CT states are commonly investigated within the two-state MLJ formalism (see ESI,† Section S4 for details).[4,21,47–49] Briefly, in the MLJ framework, both radiative and non-radiative transitions are described as electron-transfer events between the CT and ground (G) states. We neglect the transitions between charge-carrier states and CT states, as it was previously shown that carrier recombination does not contribute to the PL kinetics of the CT states.[32] Thus, this model assumes that the electronic coupling (V_{CT-G}) between the CT and G states is much larger than that between the CT state and donor and/or acceptor LE state (V_{CT-LE}). The non-radiative and radiative transition rates can then be written as a function of the adiabatic CT energy (E_{CT}), electronic coupling (V_{CT-G}), classical (λ_c) and quantum mechanical (λ_{qm}) components of the total reorganization energy ($\lambda_t = \lambda_c + \lambda_{qm}$), frequency of an effective quantum vibrational mode (ω_{qm}), and transition dipole moment (d_{CT}). The MLJ model has previously been used extensively to rationalize the experimental non-radiative voltage losses in polymer/NFA,[12,13,15,16,24,38–40] polymer/fullerene,[10,13,24,37,41,42] and OLED-based OPV materials[37] (see ESI,† Section S4 for details and further discussion on the two-state MLJ model).

In order to estimate the non-radiative decay rate constant, the microscopic parameters mentioned above have to be determined first. On the theoretical side, we started by carrying out molecular dynamics (MD) simulations to gain insight into the nano-/meso-scale morphology of the m-MTDATA:3TPYMB (Fig. 4a) blend. We then computed the energy distributions of the lowest excited CT and LE states as well as of the V_{CT-G} and V_{CT-LE} electronic couplings, by performing time-dependent DFT (TDDFT) calculations at the SRSH-ωPBE-D3/6-31G(d) level of
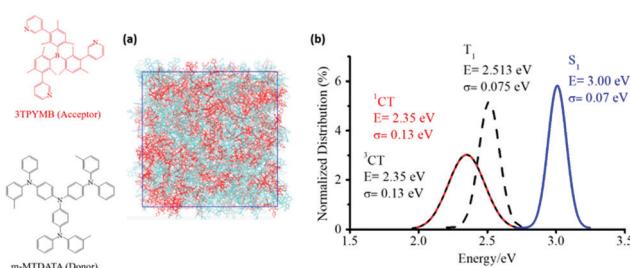
theory for 1500 D–A complexes extracted from the MD-derived film morphology. In addition, we performed geometry optimizations of the neutral and charged configurations of the m-MTDATA and 3TPYMB molecules to estimate the intra-molecular contributions to the reorganization energy λ_t. Fig. 4b shows that the singlet (^1CT) and triplet (^3CT) CT states have similar energy distributions, with the singlet–triplet energy splitting not exceeding 2 meV. The energy distribution of the lowest triplet state in the m-MTDATA molecule overlaps with the ^1CT and ^3CT distributions.[50] Since the spin–orbit coupling between pure CT states is zero,[51] the observed proximity between LE and CT states could play a significant effect on the ISC transitions between exciplex states.

Fig. 5 displays the results derived for the electronic couplings and reorganization energies. Fig. 5a and b shows that the electronic couplings between the singlet CT state and the first LE singlet excited state (V_{CT-LE}) and those between the CT state and the ground state (V_{CT-G}) have exponential-type energy distributions with average values of 3 meV for V_{CT-LE} and 6 meV for V_{CT-G}. We estimate the overall reorganization energy to be 0.41 eV, with 0.18 eV coming from the D component and 0.23 eV from the A component. As seen from Fig. 5c and d, the partition of the reorganization energy over the normal modes indicates that a significant contribution to the reorganization energy comes from low-energy (classical) vibrational modes.

On the experimental side, information on the microscopic parameters can be obtained from the intensity and profile of the absorption or emission CT band.[52–54] Here, we estimated E_{CT}, λ_t, λ_{qm} and ω_{qm} by fitting the profile of the blend PL band measured at 80 K to an extended version of the MLJ model that accounts for static disorder (see eqn (S11), ESI†). As seen from Fig. 6a (red trace), an excellent simulation of the CT band can be obtained by using: $E_{CT} = 2.65$ eV, $\lambda_t = 0.4$ eV, $\lambda_{qm} = 0.25$ eV, $\omega_{qm} = 0.1$ eV, and $\sigma_s = 70$ meV for the standard deviation of static disorder (70 meV is in the range of reported values for other D:A blends[55]). For high-energy CT systems, such as the
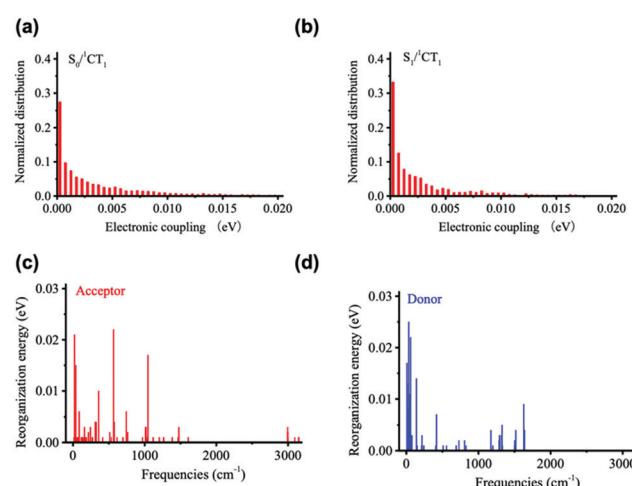
Fig. 5 Distributions of (a) V_{CT-G} and (b) V_{CT-LE} electronic couplings, and vibrational normal-mode contributions to the (c) acceptor and (d) donor reorganization energy components of λ_t.

Fig. 4 (a) Illustration of the simulated morphologies of the m-MTDATA: 3TPYMB blend. (b) Distributions of the calculated energies of the lowest CT and LE singlet and triplet states.
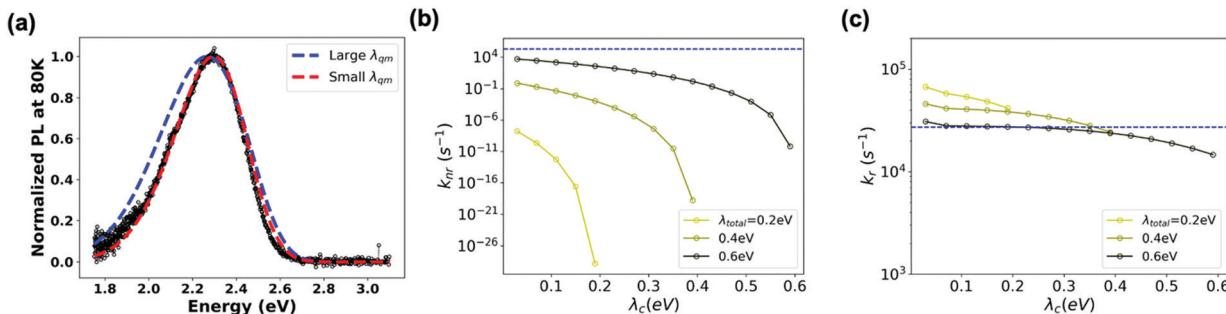
Fig. 6 (a) Comparison between the experimental PL spectrum (black) and best-fits from simulation (red and blue). λ_t is fixed at 0.4 eV, σ_s = 70 meV, ω_{qm} = 0.1 eV. Blue trace: λ_{qm} = 0.39 eV, E_{CT} = 2.58 eV; red: λ_{qm} = 0.2 eV, E_{CT} = 2.65 eV. (b) k_{nr} and (c) k_r calculated as a function of total reorganization energy, using the following microscopic parameters: σ_s = 70 meV, ω_{qm} = 0.1 eV, and E_{CT} = 2.58 eV. For each curve, the total reorganization energy shown in the legend is fixed at a certain value (0.2 eV, 0.4 eV, 0.6 eV) and the portion accounted to λ_c (up to 100% λ_t with the balance being λ_{qm}) is varied as indicated on the x-axis. The blue dotted line is the experimental value.

TADF-based system in this study and OLED-material-based systems, the non-radiative transition rates can vary by orders of magnitude as a function of the reorganization energy (and are particularly sensitive to λ_{qm}) (see Fig. S5, ESI†). Since the MLJ fitting procedure depends on the multiple parameters listed above and thus is not unique, we checked what could be the upper limit of the reorganization energy. We found that MLJ calculations employing λ_{qm} of 0.39 eV or larger yield broader PL bands than that observed experimentally, even for negligible values of λ_c (Fig. 6a). Thus, we conclude that, in the present system, λ_{qm} must be smaller than 0.39 eV. This conclusion is in good agreement with the results of the quantum-mechanical calculations described above, which yield a value of 0.41 eV for the total reorganization energy λ_t.

We next use the Mulliken–Hush formalism to estimate the V_{CT-G} electronic coupling:[53]

$$V_{CT\text{-}G} = \frac{d_{CT\text{-}G}}{\Delta d_{CT\text{-}G}} E_{CT}^v \qquad (3)$$

where $\Delta d_{CT\text{-}G}$ is the difference between the CT and G state dipole moments. We obtained the transition dipole moment ($d_{CT\text{-}G}$ = 0.05 D) and transition (vertical) energy (E_{CT}^v = 2.16 eV) from the PL measurements (see ESI,† Section S5 for details). $\Delta d_{CT\text{-}G}$ can also be estimated experimentally via electro-absorption spectroscopy.[12,56] For the sake of simplicity, we took $\Delta d_{CT\text{-}G}$ = 23 D, as calculated at the DFT level. Based on eqn (3), we estimate a value of 5 meV for $V_{CT\text{-}G}$, which is in very good agreement with the average value of 6 meV obtained from the TDDFT calculations, as described above (see ESI,† Section S6 for details on the theoretical methodology).

Based on these parameters, we calculated k_r and k_{nr} within the MLJ framework (see ESI,† Section S4 for details). Fig. 6b and c highlight that a variation of λ_t (and λ_{qm}) in the range of 0.2–0.6 eV results in a variation of the non-radiative transition rates by many orders of magnitude, whereas the radiative transition rates exhibit a less dramatic response. Intriguingly, if we employ the microscopic parameters reported above: $V_{CT\text{-}G}$ = 0.01 eV, E_{CT} = 2.65 eV, λ_t = 0.4 eV, λ_{qm} = 0.25 eV, ω_{qm} = 0.1 eV and σ_s = 70 meV, we find that the MLJ theory estimate for k_{nr} is about 8 orders of magnitude smaller than the

experimental value. To reproduce the experimental k_{nr} value using the MLJ model would require λ_t values exceeding 0.6 eV and coming nearly exclusively from quantum vibrational modes (Fig. 6b). However, if such high λ_t were actually the case, the MLJ model predicts that the PL emission spectrum would be significantly broader and shifted from the experimental absorption spectrum. Since the actual situation is inconsistent with this picture, we must conclude that the MLJ framework is unable to provide a self-consistent description of the transition rates and PL spectrum of the m-MTDATA: 3TPYMB blend. More importantly, this crosschecking exercise again highlights the importance of using the appropriate microscopic parameters, especially reorganization energy, when predicting CT kinetics and thus non-radiative voltage loss: While it may be possible to fit spectra and rates, doing so with unphysical molecular parameters would not provide the sought-after physical insight.

Three-state model

From this discussion, it is not surprising that high-energy CT systems could exhibit very small non-radiative decay rates. For the m-MTDATA:3TPYMB blend, the question in fact is why the experimental non-radiative rate is dramatically faster than that expected in the framework of the MLJ model, even though it appears much slower than most of the reported values for (lower energy) organic CT states. Finding the explanation requires going beyond the two-state model. Since the local exciton states formed on m-MTDATA and 3TPYMB efficiently dissociate into CT states, it means that that the LE and CT states are also electronically coupled. According to our DFT calculations, the coupling between the CT state and lowest LE state ($V_{CT\text{-}LE}$) is about 3 meV. We have previously shown that a three-state model, which accounts for the couplings of the CT state with both the LE and ground states, is needed in order to rationalize the radiative and non-radiative transitions from inter-molecular and intra-molecular CT states.[57] In fact, as we have recently found in the case of D–A neutral radical systems, when the LE state exhibits large non-radiative rates, even a modest hybridization between the LE and CT states can result in a significant increase in the CT k_{nr} value.[58] The experimental

optical-gap (adiabatic) energies (E_{LE}) are 3.09 eV in m-MTDATA and 3.5 eV in 3TPYMB (see ESI,† Section S3). The k_{nr} value for the CT state when considering CT-LE hybridization can be roughly estimated as:[58,59]

$$k_{nr} = (1 - f_{CT\text{-}LE})k_{nr}^{MLJ} + f_{CT\text{-}LE}k_{nr}^{LE} \qquad (4)$$

$$f_{CT\text{-}LE} = \left[\frac{V_{CT\text{-}LE}}{\Delta E_{LE\text{-}CT}}\right]^2 \bigg/ \left(1 + \left[\frac{V_{CT\text{-}LE}}{\Delta E_{LE\text{-}CT}}\right]^2\right) \qquad (5)$$

where k_{nr} is the non-radiative rate for the CT state in the three-state model, k_{nr}^{MLJ} is the non-radiative rate for the CT state according to MLJ two-state theory, k_{nr}^{LE} is the non-radiative rate for the LE state according to MLJ theory, $f_{CT\text{-}LE}$ describes the contributions of k_{nr}^{LE} to k_{nr}, and $\Delta E_{LE\text{-}CT}$ is the difference between the adiabatic LE and CT energies.

Using the experimental k_{nr}^{LE} rates for m-MTDATA and 3TPYMB, the experimental optical-gap (adiabatic) energy (see ESI,† Section S3), and the DFT electronic coupling between the CT and LE states (assuming that this coupling is the same for both m-MTDATA and 3TPYMB), we estimate that CT-LE mixing leads to an increase in k_{nr} by a factor of about $3 \times 10^4 \text{ s}^{-1}$; this value is in very good qualitative agreement with the experimental value of $9.8 \times 10^4 \text{ s}^{-1}$. To rationalize the k_r value in the context of the three-state model, a similar procedure can be performed for the transition dipole moments:[60,61]

$$(d_r^{CT})^2 = (1 - f_{CT\text{-}LE})(d_{CT\text{-}G})^2 + f_{CT\text{-}LE}(d_r^{LE})^2 \qquad (6)$$

The derived transition dipole moment can be then used to calculate the radiative rates by means of eqn (S8) or (S10) (ESI†). For the m-MTDATA:3TPYMB blend, the contribution to k_r from CT-LE hybridization is smaller than that due to CT-G hybridization. Thus, we conclude that the non-radiative transitions in the m-MTDATA:3TPYMB blend are governed by the coupling of the CT states with the LE states while the radiative decay of the CT state is dominated by the CT-G coupling.

These findings for the m-MTDATA:3TPYMB system indicate that in D:A blends with CT energies above 2 eV, the PLQY of the blend can be much larger than the PLQY values of the pristine D and A components as a result of the very small intrinsic non-radiative rates of the CT states. However, the blend's PLQY can be negatively affected by CT-LE mixing since the large k_{nr} value of the LE state can significantly speed up the CT-state k_{nr}. Overall, what these results tell us is that a strong hybridization between the CT and ground states, and a weak hybridization between the CT and LE states can result in blends with very large PLQYs even for D and A components with moderate individual PLQY values.

This phenomenon is in stark contrast with what is found in donor/acceptor blends commonly used for OPV applications. According to the Shockley–Queisser model, to obtain highly efficient solar cells, the bandgap (and hence CT-state energies) should be in the range of 1.0–1.6 eV.[1] In such instances, the CT non-radiative rates are significant. Thus, in order to minimize the non-radiative voltage loss, CT-LE mixing with an LE state having a high PLQY is beneficial, in such a way that the CT-state emission can "borrow intensity" from the LE state.[3,24,57] A small LE-CT energy gap is then desirable in this case.[24]

In order to better illustrate the effect of CT-LE hybridization over a range of CT energies, we calculated the blend's (CT) PLQY as a function of LE-CT energy (Fig. 7, red trace). In this calculation, the electronic couplings between the CT states and the ground and LE states ($V_{CT\text{-}G}$ and $V_{CT\text{-}LE}$), the transition dipole moment ($d_{CT\text{-}G}$, estimated according to eqn (3)), the LE adiabatic energy (E_{LE}), and the LE radiative and non-radiative rates (k_r^{LE} and k_{nr}^{LE}) are fixed as given in the Fig. 7 caption. In the two-state model (Fig. 7, black trace), the blend's PLQY saturates when E_{CT} approaches 2 eV because k_{nr} is significantly smaller than k_r. In the three-state model, however, the maximum PLQY of the blend is obtained at CT energies of about 2 eV. When the adiabatic energy of the CT state approaches that of the LE states, the CT-LE hybridization becomes "activated" and the LE-state large k_{nr} value carries over to the CT k_{nr} (Fig. 7b), which reduces the blend's PLQY.

Recent OPV studies concluded that in the context of CT-LE mixing, the LE PLQY sets an upper limit for the CT PLQY. We wondered whether this holds true in the case of high-gap blends, where the LE k_{nr} contributes significantly to the CT k_{nr}. We calculated the CT transition rates and PLQY, while keeping $PLQY_{LE}$ fixed at 10% but considering a range of values for the LE lifetimes (τ_{LE}). Fig. 7 shows that τ_{LE} can affect the blend's PLQY. Specifically, when τ_{LE} becomes longer, the
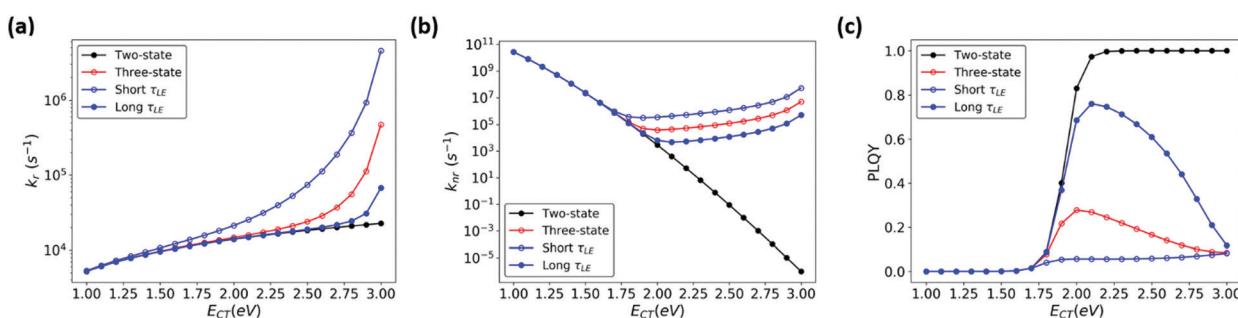
Fig. 7 (a) k_r (b) k_{nr}, and (c) PLQY calculated for a range of E_{CT} values, based on two-state MLJ (black) and three-state models (blue and red). The red line represents results based on a three-state model using the LE lifetime (Table S1, ESI,† τ_{LE} = 2.12 ns), while the blue traces represent results from three-state model calculations where τ_{LE} was increased (shown in solid circles) or decreased (shown in open circles) by 10-fold, by manipulating k_r and k_{nr} simultaneously. Parameters used: E_{CT} = 1.0–3.0 eV, $V_{CT\text{-}G}$ = 10 meV and $V_{CT\text{-}LE}$ = 10 meV, $d_{CT\text{-}G}$ = 0.049 D, d_r^{LE} = 3.58 D, k_{nr}^{LE} = $4.2 \times 10^8 \text{ s}^{-1}$, k_r^{LE} = $5.14 \times 10^7 \text{ s}^{-1}$ are based on parameters for pure m-MTDATA and the blend (Table S1, ESI†).

blend's PLQY increases (Fig. 7c, solid blue circles), whereas a shorter τ_{LE} (open blue circles) leads to smaller PLQY of the blend. Furthermore, we evaluated the influence of $PLQY_{LE}$ on the blend (ESI,† Section S7). In this series of calculations, we increased k_r^{LE} or decreased k_{nr}^{LE} to obtain a higher $PLQY_{LE}$ (80%) (Fig. S9, ESI†). The blend's (CT) PLQY maximizes when $PLQY_{LE}$ is increased by reducing k_{nr}^{LE} rather than increasing k_r^{LE}. Here as well, a longer τ_{LE} is beneficial for the blend's PLQY at higher CT energies. Finally, we show in Fig. S10 and S11 (ESI†) that a moderate change of the electronic couplings has little effect on the CT PLQY. Thus, for blends with large LE PLQY values, the CT PLQY increases systematically with an increase in CT energy. This finding is in line with the data obtained for blends where, upon blend dilution, the blend emission energy and PLQY increase concomitantly.[62,63]

Conclusions

In summary, we have demonstrated that a highly emissive and charge-generating organic photovoltaic blend based on a TADF-emitting CT state can exhibit an extremely small non-radiative recombination loss, ΔV_{OC}^{nr}, of only ~ 0.1 V and a photocurrent EQE_{max} of 24%. Compared to previously reported OPV blends, this model system demonstrates an extremely slow non-radiative recombination rate of 9.8×10^4 s^{-1}, approximately 4 to 5 orders of magnitude slower than in typical efficient polymer/NFA blends.

In this context, we re-examined the "Energy Gap Law" for non-radiative voltage loss by using the two-state Marcus–Levich–Jortner approach[20] and tuning the molecular parameters such as reorganization energy and change in dipole moment. We find that, for values of reorganization energies that are consistent with the spectral lineshapes in the MLJ picture, the non-radiative recombination rate in our blend is much faster than the MLJ model estimates.

As a result, we conclude that a three-state model that includes the local exciton state in addition to the CT and ground states is required to understand our observations. We show that the hybridization between the CT and LE states, which was previously considered to enhance only the radiative decay rates of the CT states (via intensity borrowing), can in fact also speed up the non-radiative decay, thus compromising the CT PLQY. Furthermore, in the context of the three-state model, for organic blends with CT energies over 2.0 eV, to achieve an optimal PLQY requires not only choosing low-gap components with a high PLQY, but also an evaluation of how the k_r and k_{nr} rates from the LE states tune the CT PLQY via CT-LE mixing. This consideration must inform the material selection for high-gap CT-based OLEDs.

Conflicts of interest

There are no conflicts to declare.

Acknowledgements

Notes and references

1 W. Shockley and H. J. Queisser, *J. Appl. Phys.*, 1961, **32**, 510–519.

2 O. D. Miller, E. Yablonovitch and S. R. Kurtz, *IEEE J. Photovoltaics*, 2012, **2**, 303–311.

3 V. Coropceanu, X.-K. Chen, T. Wang, Z. Zheng and J.-L. Brédas, *Nat. Rev. Mater.*, 2019, **4**, 689–707.

4 X. Liu, Y. Li, K. Ding and S. Forrest, *Phys. Rev. Appl.*, 2019, **11**, 024060.

5 Y. Xie and H. Wu, *Mater. Today Adv.*, 2020, **5**, 100048.

6 I. L. Braly, D. W. Dequilettes, L. M. Pazos-Outón, S. Burke, M. E. Ziffer, D. S. Ginger and H. W. Hillhouse, *Nat. Photonics*, 2018, **12**, 355–361.

7 D. W. Dequilettes, S. Koch, S. Burke, R. K. Paranji, A. J. Shropshire, M. E. Ziffer and D. S. Ginger, *ACS Energy Lett.*, 2016, **1**, 438–444.

8 M. A. Green, E. D. Dunlop, J. Hohl-Ebinger, M. Yoshita, N. Kopidakis and A. W. Y. Ho-Baillie, *Prog. Photovoltaics Res. Appl.*, 2020, **28**, 3–15.

9 J. J. Yoo, S. Wieghold, M. C. Sponseller, M. R. Chua, S. N. Bertram, N. T. P. Hartono, J. S. Tresback, E. C. Hansen, J. P. Correa-Baena, V. Bulović, T. Buonassisi, S. S. Shin and M. G. Bawendi, *Energy Environ. Sci.*, 2019, **12**, 2192–2199.

10 J. Benduhn, K. Tvingstedt, F. Piersimoni, S. Ullbrich, Y. Fan, M. Tropiano, K. A. McGarry, O. Zeika, M. K. Riede, C. J. Douglas, S. Barlow, S. R. Marder, D. Neher, D. Spoltore and K. Vandewal, *Nat. Energy*, 2017, **2**, 17053.

11 N. An, Y. Cai, H. Wu, A. Tang, K. Zhang, X. Hao, Z. Ma, Q. Guo, H. S. Ryu, H. Y. Woo, Y. Sun and E. Zhou, *Adv. Mater.*, 2020, **2002122**, 1–7.

12 M. E. Ziffer, S. B. Jo, H. Zhong, L. Ye, H. Liu, F. Lin, J. Zhang, X. Li, H. W. Ade, A. K.-Y. Jen and D. S. Ginger, *J. Am. Chem. Soc.*, 2018, **140**, 9996–10008.

13 S. Liu, J. Yuan, W. Deng, M. Luo, Y. Xie, Q. Liang, Y. Zou, Z. He, H. Wu and Y. Cao, *Nat. Photonics*, 2020, **14**, 300–305.

14 Y. Cui, H. Yao, J. Zhang, T. Zhang, Y. Wang, L. Hong, K. Xian, B. Xu, S. Zhang, J. Peng, Z. Wei, F. Gao and J. Hou, *Nat. Commun.*, 2019, **10**, 2515.

15 D. Qian, Z. Zheng, H. Yao, W. Tress, T. R. Hopper, S. Chen, S. Li, J. Liu, S. Chen, J. Zhang, X.-K. Liu, B. Gao, L. Ouyang, Y. Jin, G. Pozina, I. A. Buyanova, W. M. Chen, O. Inganäs, V. Coropceanu, J.-L. Bredas, H. Yan, J. Hou, F. Zhang, A. A. Bakulin and F. Gao, *Nat. Mater.*, 2018, **17**, 703–709.

16 X. Liu, X. Du, J. Wang, C. Duan, X. Tang, T. Heumueller, G. Liu, Y. Li, Z. Wang, J. Wang, F. Liu, N. Li, C. J. Brabec, F. Huang and Y. Cao, *Adv. Energy Mater.*, 2018, **8**, 1–9.

17 Y. Cui, H. Yao, J. Zhang, K. Xian, T. Zhang, L. Hong, Y. Wang, Y. Xu, K. Ma, C. An, C. He, Z. Wei, F. Gao and J. Hou, *Adv. Mater.*, 2020, **1908205**, 1–7.

18 T. Kirchartz, U. Rau, M. Kurth, J. Mattheis and J. H. Werner, *Thin Solid Films*, 2007, **515**, 6238–6242.

19 R. Engleman and J. Jortner, *Mol. Phys.*, 1970, **18**, 145–164.

20 M. Azzouzi, J. Yan, T. Kirchartz, K. Liu, J. Wang, H. Wu and J. Nelson, *Phys. Rev. X*, 2018, **8**, 1–14.

21 F. J. Kahle, A. Rudnick, H. Bässler and A. Köhler, *Mater. Horiz.*, 2018, **5**, 837–848.

22 M. Panhans, S. Hutsch, J. Benduhn, K. S. Schellhammer, V. C. Nikolis, T. Vangerven, K. Vandewal and F. Ortmann, *Nat. Commun.*, 2020, **11**, 1–10.

23 D. Qian, Z. Zheng, H. Yao, W. Tress, T. R. Hopper, S. Chen, S. Li, J. Liu, S. Chen, J. Zhang, X. K. Liu, B. Gao, L. Ouyang, Y. Jin, G. Pozina, I. A. Buyanova, W. M. Chen, O. Inganäs, V. Coropceanu, J. L. Bredas, H. Yan, J. Hou, F. Zhang, A. A. Bakulin and F. Gao, *Nat. Mater.*, 2018, **17**, 703–709.

24 F. D. Eisner, M. Azzouzi, Z. Fei, X. Hou, T. D. Anthopoulos, T. J. S. Dennis, M. Heeney and J. Nelson, *J. Am. Chem. Soc.*, 2019, **141**, 6362–6374.

25 G. Giro, M. Cocchi, J. Kalinowski, P. Di Marco and V. Fattori, *Chem. Phys. Lett.*, 2000, **318**, 137–141.

26 M. Zhang, C. Zheng, H. Lin and S.-L. Tao, *Mater. Horiz.*, 2021, **8**, 401–425.

27 S. M. King, S. I. Hintschich, D. Dai, C. Rothe and A. P. Monkman, *J. Phys. Chem. C*, 2007, **111**, 18759–18764.

28 X. Chen, D. Kim and J. Bredas, *Acc. Chem. Res.*, 2018, **51**, 2215–2224.

29 J. Gibson, A. P. Monkman and T. J. Penfold, *ChemPhysChem*, 2016, 2956–2961.

30 P. L. Santos, F. B. Dias and A. P. Monkman, *J. Phys. Chem. C*, 2016, **120**, 18259–18267.

31 K. Goushi, K. Yoshida, K. Sato and C. Adachi, *Nat. Photonics*, 2012, **6**, 253–258.

32 P. B. Deotare, W. Chang, E. Hontz, D. N. Congreve, L. Shi, P. D. Reusswig, B. Modtland, M. E. Bahlke, C. K. Lee, A. P. Willard, V. Bulovic, T. Van Voorhis and M. A. Baldo, *Nat. Mater.*, 2015, **14**, 1130–1134.

33 W. Chang, D. N. Congreve, E. Hontz, M. E. Bahlke, D. P. Mcmahon, T. Van Voorhis, M. A. Baldo, S. Reineke, T. C. Wu and V. Bulovic, *Nat. Commun.*, 2015, 1–6.

34 N. Bunzmann, S. Weissenseel, L. Kudriashova, J. Gruene, B. Krugmann, J. V. Grazulevicius, A. Sperlich and V. Dyakonov, *Mater. Horiz.*, 2020, **7**, 1126–1137.

35 D. B. Sulas, E. J. Rabe and C. W. Schlenker, *J. Phys. Chem. C*, 2017, **121**, 26667–26676.

36 S. J. Byrnes, 2018, arXiv 1603.02720v3, 1–20.

37 S. Ullbrich, J. Benduhn, X. Jia, V. C. Nikolis, K. Tvingstedt, F. Piersimoni, S. Roland, Y. Liu, J. Wu, A. Fischer, D. Neher, S. Reineke, D. Spoltore and K. Vandewal, *Nat. Mater.*, 2019, **18**, 459–464.

38 W. Zhao, D. Qian, S. Zhang, S. Li, O. Inganäs, F. Gao and J. Hou, *Adv. Mater.*, 2016, **28**, 4734–4739.

39 J. Zhang, B. Kan, A. J. Pearson, A. J. Parnell, J. F. K. Cooper, X. K. Liu, P. J. Conaghan, T. R. Hopper, Y. Wu, X. Wan, F. Gao, N. C. Greenham, A. A. Bakulin, Y. Chen and R. H. Friend, *J. Mater. Chem. A*, 2018, **6**, 18225–18233.

40 J. Liu, S. Chen, D. Qian, B. Gautam, G. Yang, J. Zhao, J. Bergqvist, F. Zhang, W. Ma, H. Ade, O. Inganäs, K. Gundogdu, F. Gao and H. Yan, *Nat. Energy*, 2016, **1**, 16089–16095.

41 N. A. Ran, J. A. Love, C. J. Takacs, A. Sadhanala, J. K. Beavers, S. D. Collins, Y. Huang, M. Wang, R. H. Friend and G. C. Bazan, *Adv. Mater.*, 2016, 1482–1488.

42 C. Wang, X. Xu, W. Zhang, J. Bergqvist, Y. Xia, X. Meng, K. Bini, W. Ma, A. Yartsev, K. Vandewal, M. R. Andersson, O. Inganäs, M. Fahlman and E. Wang, *Adv. Energy Mater.*, 2016, **6**, 1–10.

43 U. Rau, *Phys. Rev. B: Condens. Matter Mater. Phys.*, 2007, **76**, 1–8.

44 U. Rau, B. Blank, T. C. M. Müller, T. Kirchartz and F. Jülich, *Phys. Rev. Appl.*, 2017, 044016.

45 D. Baran, T. Kirchartz, S. Wheeler, S. Dimitrov, M. Abdelsamie, J. Gorman, R. S. Ashraf, S. Holliday, A. Wadsworth, N. Gasparini, P. Kaienburg, H. Yan, A. Amassian, C. J. Brabec, J. R. Durrant and I. Mcculloch, *Energy Environ. Sci.*, 2016, **9**, 3783–3793.

46 S. Ullbrich, J. Benduhn, X. Jia, V. C. Nikolis, K. Tvingstedt, F. Piersimoni, S. Roland, Y. Liu, J. Wu, A. Fischer, D. Neher, S. Reineke, D. Spoltore and K. Vandewal, *Nat. Mater.*, 2019, **18**, 459–464.

47 J. Jortner, *J. Chem. Phys.*, 1976, **64**, 4860–4867.

48 M. Azzouzi, J. Yan, T. Kirchartz, K. Liu, J. Wang, H. Wu and J. Nelson, *Phys. Rev. X*, 2018, **8**, 031055.

49 T. Wang, V. Coropceanu and J.-L. Brédas, *Chem. Mater.*, 2019, **31**, 6239–6248.

50 Z. Zheng, N. R. Tummala, Y. T. Fu, V. Coropceanu and J. L. Brédas, *ACS Appl. Mater. Interfaces*, 2017, **9**, 18095–18102.

51 B. T. Lim, S. Okajima, A. K. Chandra and E. C. Lim, *Chem. Phys. Lett.*, 1981, **79**, 22–27.

52 N. S. Hush, *Electrochim. Acta*, 1968, **13**, 1005–1023.

53 N. S. Hush, *Prog. Inorg. Chem.*, 1967, **8**, 391–444.

54 R. S. Mulliken, *J. Am. Chem. Soc.*, 1952, **74**, 811–824.

55 T. M. Burke, S. Sweetnam, K. Vandewal and M. D. McGehee, *Adv. Energy Mater.*, 2015, **5**, 1500123.

56 D. H. Oh, M. Sano and S. G. Boxer, *J. Am. Chem. Soc.*, 1991, **113**, 6880–6890.

57 X.-K. Chen, V. Coropceanu and J.-L. Brédas, *Nat. Commun.*, 2018, **9**, 5295.

58 E. Cho, V. Coropceanu and J. L. Brédas, *J. Am. Chem. Soc.*, 2020, **142**, 17782–17786.

59 I. R. Gould and S. Farid, *J. Phys. Chem. B*, 2007, **111**, 6782–6787.

60 M. Bixon, J. Jortner, J. Cortes, H. Heitele and M. E. Michel-Beyerle, *J. Phys. Chem.*, 1994, **98**, 7289–7299.

61 M. Bixon, J. Jortner and J. W. Verhoeven, *J. Am. Chem. Soc.*, 1994, **116**, 7349–7355.

62 M. Chapran, P. Pander, M. Vasylieva, G. Wiosna-Salyga, J. Ulanski, F. B. Dias and P. Data, *ACS Appl. Mater. Interfaces*, 2019, **11**, 13460–13471.

63 M. Colella, A. Danos and A. P. Monkman, *J. Phys. Chem. Lett.*, 2019, **10**, 793–798.